PAPER

Impact of electron-captures on nuclei near $N = 50$ on core-collapse supernovae

IOP Publishing Journal of Physics G: Nuclear and Particle Physics
J. Phys. G: Nucl. Part. Phys. **45** (2018) 014004 (15pp) https://doi.org/10.1088/1361-6471/aa98c1

Impact of electron-captures on nuclei near $N = 50$ on core-collapse supernovae

R Titus[1,2,3,4], C Sullivan[1,2,3], R G T Zegers[1,2,3], B A Brown[1,2,3] and B Gao[1,3]

[1] National Superconducting Cyclotron Laboratory, Michigan State University, East Lansing, MI 48824, United States of America
[2] Department of Physics and Astronomy, Michigan State University, East Lansing, MI 48824, United States of America
[3] Joint Institute for Nuclear Astrophysics: Center for the Evolution of the Elements, Michigan State University, East Lansing, MI 48824, United States of America

E-mail: taverner@nscl.msu.edu

Received 17 May 2017, revised 3 November 2017
Accepted for publication 7 November 2017
Published 13 December 2017

Abstract

The sensitivity of the late stages of stellar core collapse to electron-capture rates on nuclei is investigated, with a focus on electron-capture rates on 74 nuclei with neutron number close to 50, just above doubly magic ^{78}Ni. It is demonstrated that variations in key characteristics of the evolution, such as the lepton fraction, electron fraction, entropy, stellar density, and in-fall velocity are about 50% due to uncertainties in the electron-capture rates on nuclei in this region, although thousands of nuclei are included in the simulations. The present electron-capture rate estimates used for the nuclei in this high-sensitivity region of the chart of isotopes are primarily based on a simple approximation, and it is shown that the estimated rates are likely too high, by an order of magnitude or more. Electron-capture rates based on Gamow–Teller strength distributions calculated in microscopic theoretical models will be required to obtain better estimates. Gamow–Teller distributions extracted from charge-exchange experiments performed at intermediate energies serve to guide the development and benchmark the models. A previously compiled weak-rate library that is used in the astrophysical simulations was updated as part of the work presented here, by adding additional rate tables for nuclei near stability for mass numbers between 60 and 110.

Keywords: electron-capture rates, weak-rate library, core-collapse supernovae

(Some figures may appear in colour only in the online journal)

[4] Author to whom any correspondence should be addressed.

1. Introduction

Electron captures on nuclei play an important role in astrophysical phenomena, such as during carbon burning and later stages in massive stars [1, 2], especially the growth of the iron core [3, 4] and the subsequent collapse of the iron core leading to a core-collapse supernova [5–10], thermonuclear supernovae [11–14], neutron stars and their crusts [15, 16], and neutron-star mergers [17]. Therefore, it is important to obtain accurate nuclear-physics inputs that can be used in astrophysical simulations, including sets of electron-capture and β-decay rates across a range of stellar temperatures and densities for a large number of nuclei.

Electron-capture rates depend sensitively on the Gamow–Teller transition ($\Delta L = 0$, $\Delta S = 1$, $\Delta J = 1$) strength distribution in the β^+ direction. β^+ and electron-capture decay experiments yield the Gamow–Teller strength distributions necessary to calculate electron-capture rates [18–21]. However, these experiments are energetically limited to states within a specific Q-value window, if energetically possible at all. On the neutron-rich side of the valley of stability, decay proceeds in the β^- direction and the Gamow–Teller transitions required to calculate electron-capture rates cannot be measured with the exception of ground-state to ground-state transitions.

Charge-exchange experiments, which provide an indirect way to extract the relevant Gamow–Teller strengths, are not limited by this Q-value window. Information about transitions to higher excitation energies can be gathered across the chart of nuclides. Because of the well-established proportionality between Gamow–Teller strength and charge-exchange reaction cross section [22–24], Gamow–Teller strengths can be extracted model-independently. Therefore, charge-exchange experiments in the β^+ direction have become an important tool to extract Gamow–Teller strengths of relevance for the determination of astrophysical electron-capture rates.

Unfortunately, it is not possible to measure Gamow–Teller strength distributions on all nuclei that play a role in the above astrophysical phenomena. In addition, in high-temperature stellar environments, low-lying states in parent nuclei can be thermally populated, and electron captures can take place on these excited states [25]. Moreover, at high temperatures, shell orbits that would be Pauli-blocked at $T = 0$, can become partially unblocked [26], which changes the Gamow–Teller strength distribution. These effects are very difficult to study in the laboratory. Consequently, the electron-capture rate calculations and the astrophysical simulations can use rates determined on the basis of experiment, where available and appropriate, but in general must rely on theoretical estimates. An important role of the experiments is then to guide and benchmark the theoretical calculations and provide measures for uncertainties in the theory.

The earliest set of theoretical weak-rates, based on a single-particle estimate, were provided by Fuller, Fowler and Newman (FFN) [27–30]. With the advent of increased computational power, electron-capture rate sets based on shell-model calculations became feasible, starting with nuclei in the *sd*-shell [31], which were recently updated [2]. Weak-rate sets for nuclei in the *pf*-shell were generated [13, 25, 32] based on the KB3G interaction [33] and, recently, the GXPF1 family of interactions [34–36]. For heavier nuclei, shell-model calculations are computationally challenging, although calculations with severely constrained model spaces, such as the ^{88}Sr core, used in [37], have been used to estimate weak rates for astrophysical purposes. Consequently, other theoretical techniques, such as QRPA [38–42] or shell-model Monte-Carlo [43, 44], are used. Such calculations cannot reproduce the details of the Gamow–Teller strength distributions as well as shell-model calculations can, but at higher stellar densities (in excess of 10^{10} g cm^{-3}), such details matter somewhat less than at low densities [18].

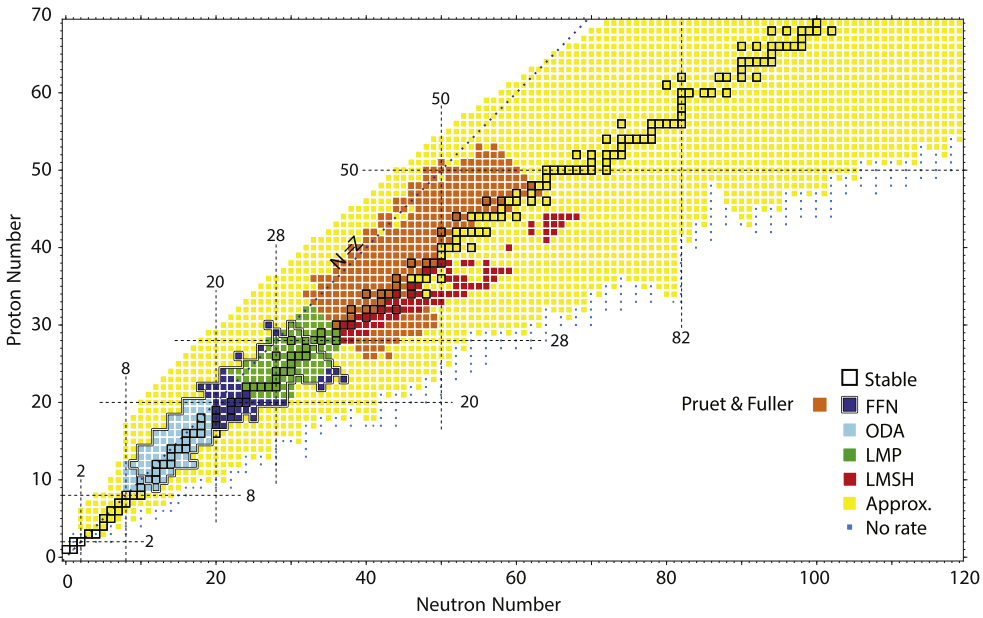

Figure 1. Nuclear species currently included in the weak-rate library. The original tables included in the library by Sullivan *et al* were FFN [28], ODA [31], LMP [32, 46] and LMSH [6, 26]. The Pruet and Fuller tables [47] were added to the library as part of the present work. Reproduced from [9]. © 2016. The American Astronomical Society. All rights reserved.

In order to consolidate all available tables of weak rates for use in astrophysical simulations, a weak-rate library was developed by Sullivan *et al* [9]. As shown in figure 1, weak rates based on microscopic calculations of varying origin cover low- and medium-mass nuclei primarily around the valley of stability. To fill in the gaps, it is necessary to turn to more rudimentary approximations. For a vast number of nuclei, especially far away from stability, an approximate method is used to generate these electron-capture rates for use in simulations [7, 45]. The weak rate library and this approximate method will be discussed in section 2.

Sensitivity studies, in which electron-capture rates are varied within uncertainties, are helpful for gaining a better understanding of the impact on the evolution of late-stage core collapse [2, 9]. In the recent work by Sullivan *et al*, it was shown that nuclei in the upper *pf*- and *pfg*/*sdg*-shells, particularly in the region around the $N = 50$ closed neutron shell at and above ^{78}Ni (see figure 2), have the largest impact on the change in electron density (Y_e) and, thus, on the dynamical evolution of the collapse. In this work, we focus our effort on this region of important nuclei (denoted hereafter as the *high-sensitivity region*) and demonstrate the importance of constraining the electron-capture rates in this region.

2. Weak rate library

The weak-rate library [9] mentioned above includes several tables of electron-capture and β-decay rates (see figure 1) over a large density and temperature grid. It can be used independently for calculations or can be used in conjunction with the neutrino-interaction library, NuLib [48]. NuLib uses the electron-capture rates in the library to calculate neutrino/

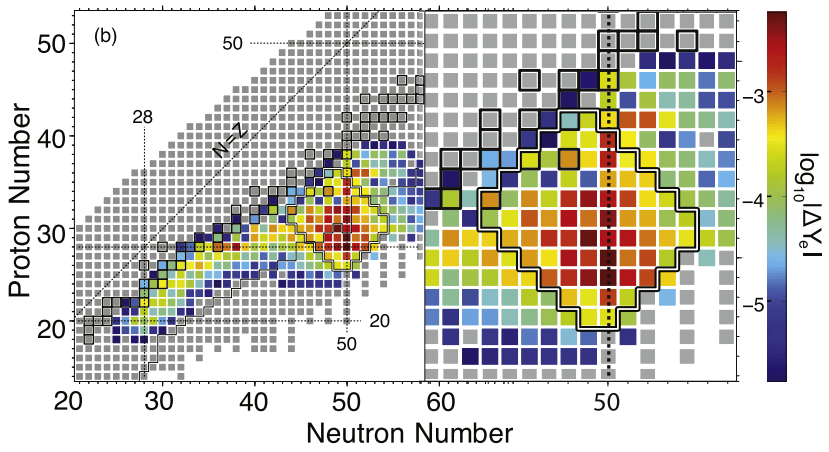

Figure 2. Contributions to the change in electron fraction (Y_e), as a function of neutron and proton number, in late stages of a core-collapse supernova, based on the work by Sullivan *et al* [9]. The right-hand side panel is zoomed into a small region of the left-hand side panel. Nuclei in this *high-sensitivity region* around $N = 50$, at and above ^{78}Ni, as outlined in both panels, are particularly important contributors to the change in Y_e and strongly affect the dynamical evolution of the supernova. Reproduced from [9].

antineutrino charged-current absorption opacities for use in astrophysical simulations. In the present work, the simulations of core-collapse supernovae are performed using the GR1D code, a general relativistic, spherically-symmetric stellar collapse code [48, 49], but the library has also been used in two-dimensional simulations of core-collapse supernovae [10].

Here, the electron-capture rates for neutron-rich nuclei far from stability in the region surrounding the $N = 50$ shell closure, and their impact on the evolution of the collapse, are examined. Many of these nuclei do not yet have an electron-capture rate based on a microscopic model calculation included in the library and, consequently, the code uses an approximate method to calculate the electron-capture rate at the appropriate density and temperature. The approximate electron-capture rate is given by [30, 46]:

$$\lambda_{\mathrm{EC}} = \frac{\ln 2 \cdot B}{K}\left(\frac{T}{m_e c^2}\right)^5 [F_4(\eta) - 2\chi F_3(\eta) + \chi^2 F_2(\eta)], \tag{1}$$

where m_e is the electron mass, $K = 6146$ s, F_k are Fermi integrals of rank k and degeneracy η, $\chi = (Q - \Delta E)/T$, $\eta = \chi + \mu_e/T$, and T and μ_e are the temperature and electron chemical potential, respectively. B, the effective Gamow–Teller transition strength, is fixed for all isotopes to 4.5. ΔE, the effective excitation energy, is fixed for all isotopes to 2.5 MeV. These values were determined in a fit to shell-model calculations for nuclei in the *pf*-shell [7] relatively close to the valley of stability. We note that, very recently, this approximate method has been improved by adjusting the effective excitation energy based on neutron and proton numbers [45] (while leaving the effective transition strength fixed).

For neutron-rich nuclei, including those in the high-sensitivity region, the use of the approximation with parameters fit to microscopic calculations for nuclei close to stability constitutes an extrapolation to a region of the chart of nuclei in which different shells play a role. Hence, the uncertainties when applying the approximation can be large, as first detailed in [44], in which occupation numbers were estimated based on predictions in shell-model

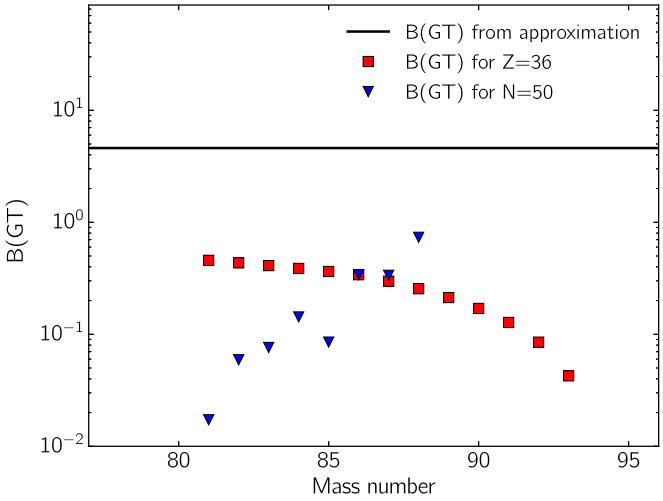

Figure 3. A comparison of Gamow–Teller strengths calculated following equation (2) and (3) [53] for nuclei on the $N = 50$ line (blue triangles), for nuclei on the $Z = 38$ line (red squares) and for the approximate method, which uses a fixed value of $B(\mathrm{GT}) = 4.6$ (black line).

Monte-Carlo calculations. At the $N = 50$ shell closure, neutrons fill the $\nu g_{9/2}$ orbital and Gamow–Teller transitions are associated with transitions in which the added neutron occupies an orbital above $\nu g_{9/2}$ [50]. Therefore, the strongest transition is $\pi g_{9/2} \rightarrow \nu g_{7/2}$ [51, 52]. If protons are present in the $\pi g_{9/2}$ orbital, the Gamow–Teller transition strength is significant. However, with increasing neutron number beyond $N = 50$, the $\nu g_{7/2}$ orbital becomes Pauli-blocked and the transition strength decreases. Similarly, as the nucleus becomes less proton-rich and the occupancy of $\pi g_{9/2}$ is lowered, the transition strength will decrease. For $N < 50$, $\pi g_{9/2} \rightarrow \nu g_{9/2}$ transitions also contribute to the Gamow–Teller transition strength.

In order to examine the effect of filling these orbitals on the Gamow–Teller strength, it is beneficial to use a simple model, using the occupancies of the $\pi g_{9/2}$, $\nu g_{7/2}$ and $\nu g_{9/2}$ orbitals. Following the work of Macfarlane [53], the Gamow–Teller strength in the β^+ direction can be estimated using:

$$S^+ = 3\sum_{nljj'}(C_{nl}^{jj'})^2(1 - n_{nlj}^N)n_{nlj'}^P, \tag{2}$$

where n_{nlj}^N is the average occupancy of the initial neutron orbital, $n_{nlj'}^P$ is the average occupancy of the final proton orbital, and

$$C_{nl}^{jj'} = [2(2j + 1)(2j' + 1)]^{1/2} W\left(l\frac{1}{2}j1; j'\frac{1}{2}\right), \tag{3}$$

in which j is the total orbital angular momentum quantum number for the initial state, j' is the total orbital angular momentum for the final state and W is the Racah W-coefficient. Here, we used the SNET interaction [52] in a model space in which protons can populate the $0f_{5/2}$, $1p_{3/2}$, $1p_{1/2}$, and $0g_{9/2}$ orbitals, and neutrons can populate the $0g_{7/2}$, $1d_{5/2}$, $1d_{3/2}$, $2s_{1/2}$ and $0h_{11/2}$ orbitals to estimate the filling of the neutron and proton orbitals.

Figure 3 shows that the Gamow–Teller strength increases with proton number along the $N = 50$ line (blue triangles). For $Z \leqslant 30$ ($A \leqslant 80$), protons do not populate the $g_{9/2}$ orbital and Gamow–Teller excitations are completely blocked. The opposite trend is seen when

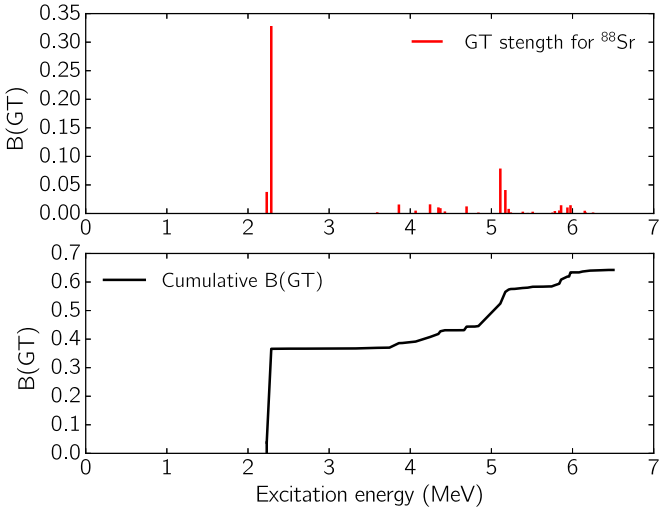

Figure 4. Gamow–Teller strength distribution for ^{88}Sr, calculated using the SNET interaction in the SNE model space [51, 52]. The cumulative Gamow–Teller strength calculated from the shell-model, shown in the bottom panel, is comparable to the value obtained from occupancy approximation of the Gamow–Teller strength, shown in figure 3. Therefore, this simple model is reasonable estimate of the total Gamow–Teller strength around the $N = 50$ shell closure.

increasing the neutron number (shown in red squares in figure 3 for the case of $Z = 36$). Below $N = 50$ ($A = 86$), $\pi g_{9/2} \rightarrow \nu g_{7/2}$ and $\pi g_{9/2} \rightarrow \nu g_{9/2}$ transitions can contribute. Above $N = 50$ ($A = 86$), $\pi g_{9/2} \rightarrow \nu g_{9/2}$ transitions are completely blocked, and $\pi g_{9/2} \rightarrow \nu g_{7/2}$ transitions increasingly so. Hence, the Gamow–Teller strength decreases, until it is completely blocked at $N = 58$ ($A = 94$) when the neutrons completely fill the $g_{7/2}$ orbital. Figure 3 also shows the strength used in the approximation of [7, 45], which is higher by approximately an order of magnitude or more in this region of the chart of isotopes than the estimates based on the orbital fillings. We note that at high stellar temperatures, thermally-driven Pauli-unblocking effects will increase the electron-capture rates beyond the value calculated at $T = 0$. For nuclei in which the Pauli-blocking effects are very strong, the unblocking can lead to a significant increase of the electron-capture rates. However, for nuclei in which the Pauli-blocking is incomplete, the effects of the increased temperatures and additional unblocking are relatively small [26]. This is the likely scenario for nuclei in the high-sensitivity region.

Ultimately, one prefers to use microscopic calculations to generate electron-capture rates based on realistic strength distributions that are benchmarked against data. In the *pf*-shell, rates calculated by using shell-models are the most accurate based on a comparison with charge-exchange data [18]. Even though shell-model calculations near $N = 50$ are a challenge, initial calculations were performed using Oxbash [54] using the SNET interaction [52]. An example of such a calculation, for the case of ^{88}Sr, is shown in figure 4. The excitation energy of the first transition in the shell-model calculation was chosen to match the first known 1^+ state in ^{88}Rb (at about 2.2 MeV), because the energy of the 2^- ground state in ^{88}Br cannot be calculated within the chosen model space.

It is found that strength extracted from the shell-occupancy approximation, discussed above, provides a similar total strength to the shell-model calculation for ^{88}Sr, indicating that

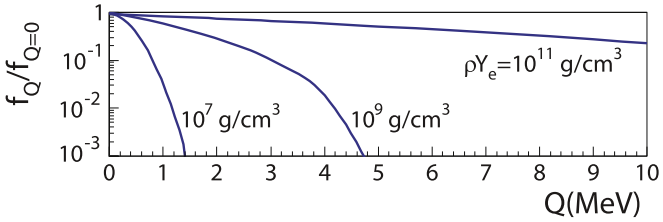

Figure 5. Phase-space factors as a function of electron-capture Q-value at stellar electron densities (ρY_e) of 10^7, 10^9, and 10^{11} g cm^{-3} respectively. The phase-space factors have been normalized to the value at $Q = 0$. The temperature was kept fixed at 10^9 K. With increasing electron density, the Fermi energy increases, and transitions to states at higher Q-value contribute more strongly.

the $\nu g_{7/2}$ and $\pi g_{9/2}$ orbitals are the dominant ones in the shell-model calculations as well. However, in the shell-model calculations, about half of the total strength is distributed over many states at higher excitation energy, which results in a reduction of the electron-capture rates compared to the assumption that all strength is contained in a single state at 2.5 MeV used in the rate approximation of equation (1). This reduction is in addition to that caused by the overestimated total transition strength. Finally, we note that it is well-known that Gamow–Teller strengths that are calculated in the shell-model must be quenched by factors of 0.5–0.6 to account for effects not included in the calculation [55–58], which reduce the total strengths and, thus, the electron-capture rates further. A quenching factor is not applied to the calculations presented in this paper.

To understand the relative importance of contributions from electron-capture transitions to final states at different Q-values, the phase-space dependence on reaction Q-value must be evaluated as a function of stellar density, as illustrated in figure 5. In this figure, the phase space factor at finite Q-value is divided by the phase-space factor at $Q = 0$, so the relative contribution (for fixed value of B(GT)) can easily be read from the figure. The stellar temperature was fixed at 10^9 K. At low stellar densities ($\rho Y_e = 10^7$ g cm^{-3}), only electron-capture transitions to states at low Q-values will contribute significantly. When the stellar density increases to $\rho Y_e = 10^9$ g cm^{-3}, the Fermi surface increases and states at higher Q-value will contribute more. At $\rho Y_e = 10^{11}$ g cm^{-3}, states at $Q \approx 10$ MeV contribute half of those close to $Q = 0$. In summary, the electron-capture rates are more sensitive to details of the Gamow–Teller strength distributions at low excitation energies and less sensitive to the total Gamow–Teller strength when the stellar density is low. The reverse is true when the density is high. The core-collapse supernova simulations performed in this work evaluate the evolution at densities above 10^{10} g cm^{-3} and fall in the latter category. When the densities are in excess of 10^{11} g cm^{-3}, contributions from forbidden transitions start to contribute as well [44, 46, 59], but they are not explicitly included here. At densities of 10^{12} g cm^{-3} the EC rate could double due to contributions from forbidden transitions [44]. Although charge-exchange experiments provide information on the strength distributions for forbidden transitions, a proportional relationship between forbidden transition strengths and charge-exchange cross sections has not been established, making it difficult to extract strengths and quantify the uncertainties in the associated electron-capture rates.

For some of the nuclei in the high-sensitivity region, electron-capture rates have been estimated by considering thermally-driven Pauli-unlocking effects in a hybrid shell-model RPA calculation [6, 26] and included in the weak-rate library. These are the rates referred to as LMSH in figure 1. A comparison between the LMSH rates and the rates based on the

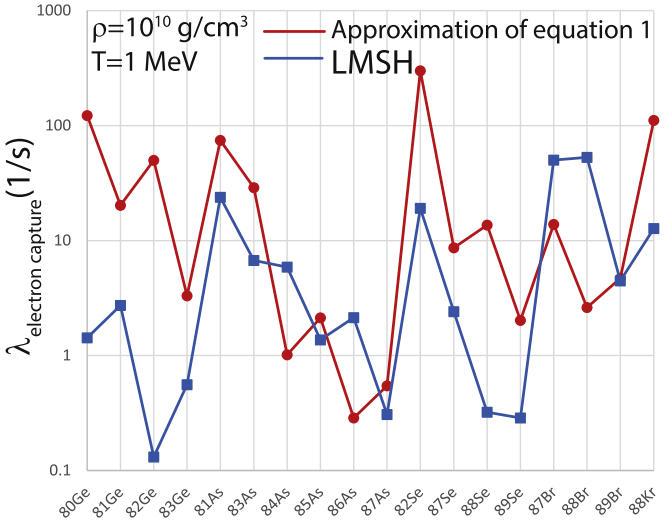

Figure 6. Comparison between electron-capture rates estimated in a hybrid shell-model RPA calculation (LMSH) [6, 26] and based on the approximation of equation (1) for nuclei in the high-sensitivity region near $N = 50$. A density of 10^{10} g cm^{-3} and a temperature of 1 MeV was used in the rate calculations.

approximation of equation (1) for nuclei in the high-sensitivity region are shown in figure 6. Because the LMSH calculations do consider the effects of Pauli blocking and have more accurate estimates for the Gamow–Teller strengths, the electron-capture rates are, generally speaking, below the estimates based on the approximation. Still, this is not uniformly the case, because the electron-capture rate Q-values used in the two methods can be different and change the estimated rates significantly. Deviations between the two methods are as large as two orders of magnitude. Clearly, guidance from charge-exchange experiments, similar to what was done for nuclei in the *pf*-shell, is required to better constrain and estimate the uncertainties in the theory and to provide data on the basis of which the theoretical estimates can be improved.

3. Addition of new tables

For the purpose of the present work, electron-capture rates, generated by Pruet and Fuller [47], were added to the weak-rate library. These rates are for a set of nuclei in the mass range $A = 66$–110 that are predominantly on the proton-rich side of the chart of nuclides and are shown by the orange squares in figure 1. The electron-capture and β^+ decay rates were calculated following the method of FFN [27]. The $A = 66$–80 section of the table covers a temperature range of 0.01–100.0 GK, and a $\log_{10}(\rho Y_e$ g cm$^{-3})$ range of 1.0–11.5. The $A = 81$–110 section of the table covers a temperature range of 0.01–1.0 GK, and a $\log_{10}(\rho Y_e$ g cm$^{-3})$ range of 1.0–7.5.

In the previous sensitivity study of core-collapse supernovae to electron-capture rates performed by Sullivan *et al* [9], the electron-capture rates for all nuclei were systematically scaled by constant factors in order to test the sensitivity of the simulations to global changes in the electron-capture rates. The inclusion of the new rate table by Pruet and Fuller did not significantly change these outcomes, primarily because the late-stage of core collapse

involves nuclei on the neutron-rich side of the valley of stability. Still, the inclusion of the new rates will be helpful for studies of other astrophysical phenomena.

4. Study of the high-sensitivity region

As discussed above and illustrated in figure 2, there is a cluster of nuclei around the $N = 50$ shell closure at and above ^{78}Ni that has a large impact on the change in electron fraction in the simulation. In order to determine the sensitivity of the simulation of the late stages of stellar collapse to this region in more detail, a set of 74 nuclei were chosen, covering both sides of the $N = 50$ line from the valley of stability to the neutron drip line, as shown in figure 2. In the study presented here, the electron-capture rates are also systematically scaled, but in addition to scaling the rates on all nuclei, simulations in which only the rates on nuclei in the high-sensitivity region are scaled, were performed. The scaling factors were chosen to represent the uncertainty in the electron-capture rates based on the comparison between different models, as discussed above, and the models and experimental data for nuclei in the *pf*-shell.

The simulation framework used for the sensitivity is the same as in Sullivan *et al* and only briefly summarized here. The open-source spherically symmetric, general-relativistic neutrino-transport and hydrodynamics code, GR1D, is used; details about the hydrodynamics are found in [49] and about the neutrino transport in [48]. In these simulations, all of the tables included in the weak-rate library were used, with the hope that a larger set of nuclei would have microphysically-accurate rate available. The electron-capture rates from the library are integrated in NuLib [48], an open-source neutrino-interaction library. A well-known 15 solar-mass, solar-metallicity progenitor (s15WW95) [60] was used in the simulations with the SFHo equation of state and nuclear statistical equilibrium distributions from [61]. It has been shown that variations in the electron-capture rates play a more important role in the simulation than variations in the progenitor or equation of state [9]. Only the electron-capture rates that were input to the simulations were changed in the sensitivity studies discussed below.

A comparison of the lepton fraction (Y_l) as a function of central density (ρ_c) for simulations in which the electron-capture rates are scaled is shown in figure 7. The black solid line represents the base calculation, in which the electron-capture rates have not been scaled. At low densities ($\rho_c \sim 10^{10}$g cm^{-3}), electron captures are responsible for the deleptonization of the matter in the core of the star. The opacity is low, allowing electron neutrinos to escape the star freely and causing the lepton fraction to decrease. When the central density reaches $\rho_c \approx 2 \times 10^{12}$ g cm^{-3}, the lepton fraction saturates (at a value of $Y_l = 0.292$ in the base calculation) because neutrino trapping prevents further deleptonization. If the electron-capture rates in the library are increased (dashed-dotted lines in figure 7), simulating the situation in which the electron-capture rates in the library are underestimated, a similar or slightly higher final lepton fraction is attained. This is due to the fact that the opacity related to electron-neutrino captures on heavy nuclei becomes stronger than opacities related to the electron-neutrino scattering, reducing the window for deleptonization to occur and preventing further deleptonization [9].

For reasons discussed above, the scenario in which the electron-capture rates in the library are overestimated is more likely. In the simulations in which the electron-capture rates are reduced (dashed ($\times$0.1) and dotted ($\times$0.01) in figure 7) the final lepton fraction significantly increases compared to the base calculation.

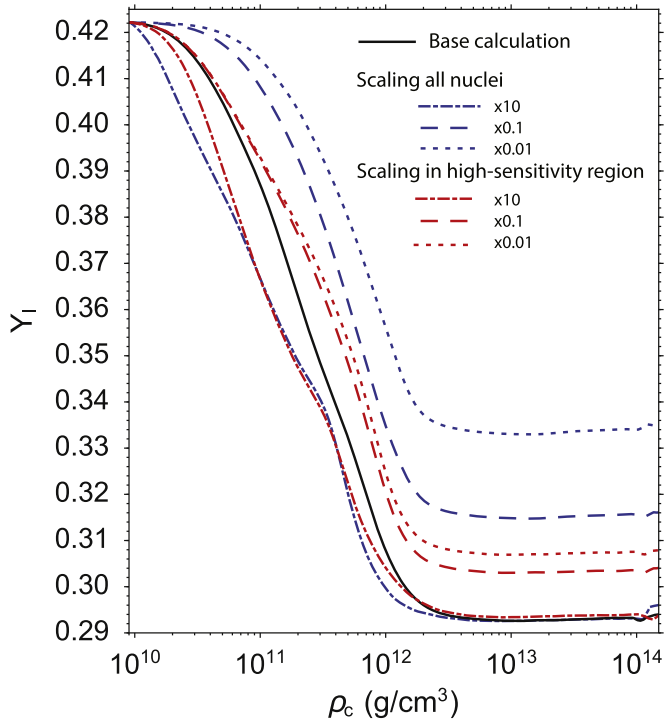

Figure 7. Diagrams of lepton fraction versus central density during the core-collapse process for different scalings of electron-capture rates for all nuclei (in red) and for nuclei in the high-sensitivity region (in blue). Scaling factors of 10, 0.1 and 0.01 are applied. The base simulation in which no rates are scaled is shown by the black line.

The blue curves in figure 7 represent scenarios in which the electron-capture rates for all nuclei in the library are scaled, whereas the red curves denote the results in which only the 74 nuclei in the high-sensitivity region are scaled. Scaling all electron-capture rates used in the simulation by a factor of 0.1 (blue dashed line) produces a final lepton fraction of ∼0.314, an increase of 7.5% compared to the base simulation. By scaling the electron-capture rates only in the high-sensitivity region (red dashed line), the final lepton fraction is ∼0.303, a 3.8% increase from the base simulation.

The relatively strong effect of scaling the electron-capture rates in the high-sensitivity region is also apparent in the simulation results for the electron fraction, entropy, stellar density and in-fall velocity at core bounce, as a function of enclosed mass, as shown in figure 8. Here, we follow the definition of t_{bounce} by the authors of GR1D, namely that it occurs when the entropy reaches a value of 3.0 [48]. The variation in simulated characteristics of these parameters, resulting from applying scaling factors of 10, 1, 0.1, and 0.01 to the electron-capture rates on the nuclei in the high-sensitivity region only is indicated by the red bands. The variation by scaling the electron-capture rates on all nuclei is indicated by the black lines. As in the case of the lepton fraction, the effect of only changing the rates for the nuclei in the high-sensitivity region accounts for the about half of the changes seen when scaling the electron-capture rates on all nuclei. Of the 8140 nuclei included in the core-collapse supernova simulations, fewer than half play a role [62] and, of these, the 74 nuclei in

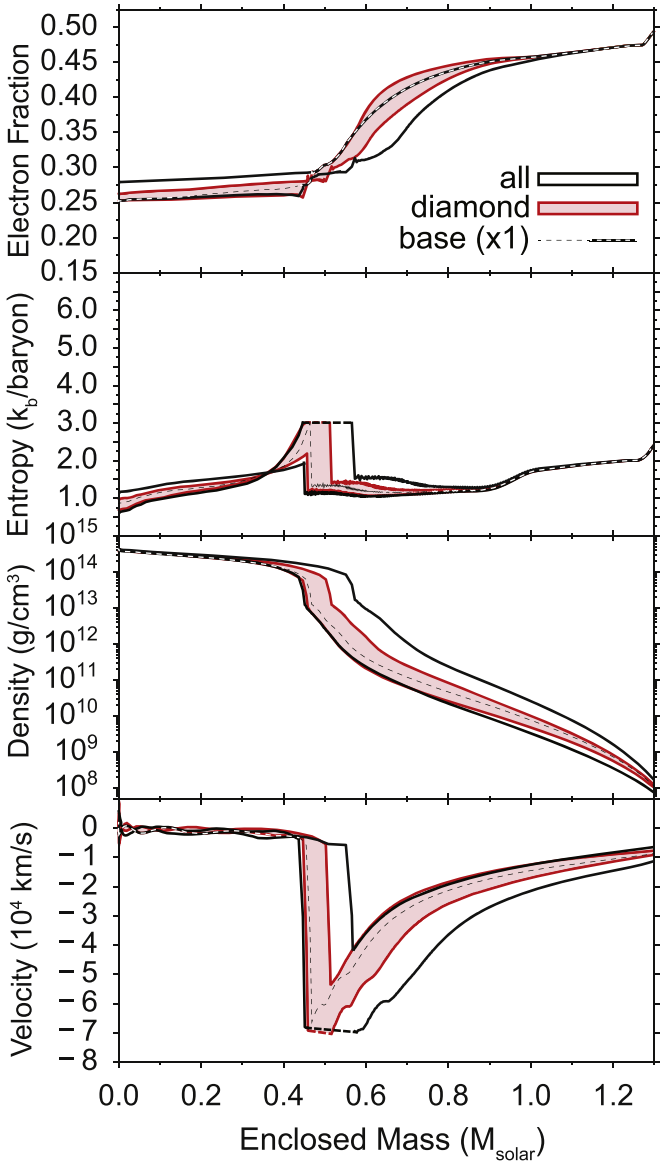

Figure 8. Electron fraction, entropy, density and matter velocity at $t = t_{\text{bounce}}$ (defined when the entropy reaches 3.0) for two sets of simulations. The bands indicate the range of values obtained when the electron capture rates are scaled in the high-sensitivity region (red) or across the entire chart of nuclides (black).

the high-sensitivity region are most important during the core-collapse and early post-bounce phases.

Figure 9 shows how much different isobars, isotopes and isotones contribute to the integrated change in electron fraction ($|\Delta Y_e|$) from the beginning of the simulation until neutrino trapping. The colors indicate the scaling factor applied to the electron-capture rates as a measure of the uncertainty into the estimated electron-capture rates used in the library. In

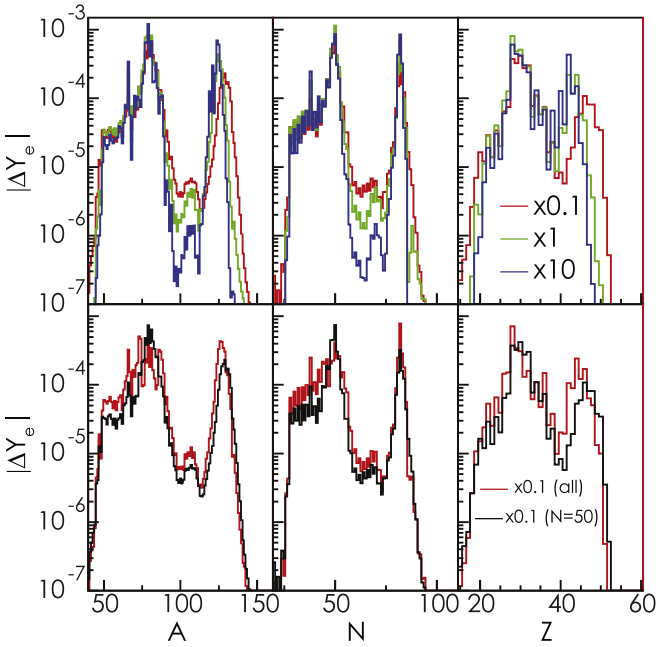

Figure 9. Integrated change in electron fraction from the beginning of the simulation until neutrino trapping. The top row shows the total electron fraction as a function of mass number, neutron number and proton number for simulations in which all electron-capture rates are scaled. Increasing the rates causes the abundance to become less proton-rich and does not affect the position of the neutron number distribution. Additionally, as the electron-capture rates are increased, the abundance tends to cluster around the closed shells, and fewer nuclei appear in the mid-shell regions. The bottom row of plots shows the simulation in which all rates are scaled by 0.1 compared to scaling the rates in the high-sensitivity region by 0.1; both cases show the abundance shifted to become less proton-rich.

the top three panels, electron-capture rates on all nuclei are scaled. In the bottom panel, distributions in which a scaling factor of 0.1 has been applied to the electron-capture rates for all nuclei (red) and in the high-sensitivity region (black) are compared. The strong contribution from nuclei near $N = 50$ to the change in electron fraction is clearly observed. A strong contribution from neutron-rich nuclei near closed-shell $N = 82$ is also obvious.

From the results in figure 9, it is observed that with decreasing electron-capture rates relative to the base rates, fewer proton-deficient nuclei play an important role in the peak at $N = 82$ ($A \sim 130$), while increasing the rates has a relatively weak impact on the overall distributions. In addition, when the electron-capture rates are decreased, the contributions to the change in electron fraction from captures on nuclei in between $N = 50$ and $N = 82$ increases, although only slightly.

By only scaling the electron-capture rates in the high-sensitivity region around $N = 50$, the trends are similar: by reducing the rates, less proton-deficient nuclei near $N = 82$ play a more important role. The observed shift in the peak near $Z = 50$ (bottom-right panel of figure 9) is about half of that observed when all rates are scaled by a factor of 0.1 (top-right panel of figure 9).

It is important to note that, although the distributions shown in figure 9 peak at $N = 50$ and $N = 82$, indicating that these groups of nuclei are predominantly responsible for the

change in electron fraction, the electron-capture on the nuclei near $N = 50$ is much more important for the simulation of the evolution of core-collapse supernovae. Simulations indicate that the nuclei at the $N = 82$ shell closure do not contribute significantly until just before core-bounce when the density is very high and neutrino trapping has already occurred. Therefore, we conclude that experimental and theoretical studies of Gamow–Teller strength distributions and derived electron-capture rates in the high-sensitivity region around $N = 50$ are the most important objective for better constraining the weak-interaction input for the purpose of simulating and for understanding the evolution of core-collapse supernovae.

5. Conclusions and outlook

From the simulations of core-collapse supernovae performed as part of this and earlier works, it has become clear that accurate electron-capture rates are very important for understanding the dynamical evolution of these cataclysmic events. Here, the focus was on the electron-capture rates on nuclei in the high-sensitivity region around $N = 50$ just above doubly-magic ^{78}Ni. Electron captures on about 74 nuclei in this region affect key characteristics, such as the lepton fraction, electron fraction, entropy, stellar density, and in-fall velocity of the evolution by as much as the other thousands of isotopes included in the simulation combined.

The electron-capture rates on nuclei in the high-sensitivity region that are currently used in the weak-rate library are probably too high because the approximation used to estimate these rates is based on microscopically calculated rates close to stability, where Pauli-blocking effects are much weaker. Although at finite stellar temperatures Pauli-unblocking occurs due to thermally-driven excitations of nuclei present in the star [41, 46], the over-estimation of the electron-capture rates could amount to an order of magnitude. In order to reduce such large uncertainties, it is important to develop better estimates which requires a combination of improved theoretical approaches and high-quality data to guide and benchmark the theoretical development. Charge-exchange experiments are used to test theoretical predictions, but, as mentioned previously, only provide information about transitions from the ground state of the parent nucleus. There are still significant uncertainties related to the effects of finite temperature corrections on electron-capture rates [41], but this is not a facet that charge-exchange experiments are able to examine.

An experimental program focused on using charge-exchange reactions at intermediate energies to measure the relevant Gamow–Teller strength distributions from the nuclei of primary interest is underway at the National Superconducting Cyclotron Laboratory, where the (t, ^{3}He) reaction is used to study transition strength from stable nuclei. The analysis of data on $N = 50$ nucleus ^{86}Kr is in progress, and an experiment focused on ^{88}Sr and ^{93}Nb is planned. These results will be combined with sparse existing data in the same mass region, which includes results from the ^{96}Mo(d, ^{2}He) [63] reaction, the ^{90}Zr(n, p) [64–66] reaction, and the ^{100}Mo(t, ^{3}He) [67] reaction. The experimental Gamow–Teller distributions will be compared with theoretical calculations, such as the shell-model calculations described in this work, as well as various density-functional calculations. It is also important to develop new experimental techniques to study Gamow–Teller transition strengths in the β^+ direction from unstable nuclei, for example by using the (d, ^{2}He) reaction in inverse kinematics.

In addition to these efforts, several improvements to the weak-rate library are ongoing. The weak-rate library used in the simulations presented in this work was expanded to contain estimated rates in the mass region between $A = 60$ and 110. Although the late-stage core collapse leading to a supernovae is not strongly affected by the inclusion of these improved rate estimates, since the nuclei included in the expansion were too proton-rich, their inclusion

will be important for studies of other astrophysical phenomena. Additional tables of electron-capture rates that have recently become available for *pf*-shell nuclei [2] will be added to the weak rate library. Finally, the approximate method for estimating weak rates based on equation (1) has been improved recently [45], by adjusting the excitation energy ΔE based on neutron and proton numbers. Although this resolves neither the issue of increased Pauli-blocking, nor the impact of fixing the strength to a value that is inconsistent with more accurate theoretical methods or with data, the new approximation provides better estimates than presently available and will be included in the library.

Acknowledgments

This work was supported by the US-NSF under grant numbers PHY-1565546 and PHY-1430152 (JINA Center for the Evolution of the Elements) and PHY-1404442. BG gratefully acknowledges the support from the China Scholarship Council (CSC). The authors also thank Dr Evan O'Connor for his support of NuLib and GR1D.

ORCID iDs

R Titus https://orcid.org/0000-0001-5362-5977

References

[1] Martínez-Pinedo G, Lam Y H, Langanke K, Zegers R G T and Sullivan C 2014 *Phys. Rev.* C **89** 045806
[2] Suzuki T, Toki H and Nomoto K 2016 *Astrophys. J.* **817** 163
[3] Heger A, Langanke K, Martínez-Pinedo G and Woosley S E 2001 *Astrophys. J.* **560** 307
[4] Heger A, Langanke K, Martínez-Pinedo G and Woosley S E 2001 *Phys. Rev. Lett.* **86** 1678
[5] Bethe H A, Brown G E, Applegate J and Lattimer J M 1979 *Nucl. Phys.* A **324** 487
[6] Hix W R, Messer O E B, Mezzacappa A, Liebendörfer M, Sampaio J, Langanke K, Dean D J and Martínez-Pinedo G 2003 *Phys. Rev. Lett.* **91** 201102
[7] Langanke K, Martínez-Pinedo G, Sampaio J M, Dean D J, Hix W R, Messer O E B, Mezzacappa A, Liebendörfer M, Janka H-T and Rampp M 2003 *Phys. Rev. Lett.* **90** 241102
[8] Janka H-T, Langanke K, Marek A, Martínez-Pinedo G and Müller B 2007 *Phys. Rep.* **442** 38
[9] Sullivan C, O'Connor E, Zegers R G T, Grubb T and Austin S M 2016 *Astrophys. J.* **816** 44
[10] Richers S, Ott C D, Abdikamalov E, O'Connor E and Sullivan C 2017 *Phys. Rev.* D **95** 063019
[11] Brachwitz F *et al* 2000 *Astrophys. J.* **536** 934
[12] Iwamoto K, Brachwitz F, Nomoto K, Kishimoto N, Umeda H, Hix W R and Thielemann F-K 1999 *Astrophys. J. Suppl. Ser.* **125** 439
[13] Mori K, Famiano M A, Kajino T, Suzuki T, Hidaka J, Honma M, Iwamoto K, Nomoto K and Otsuka T 2016 *Astrophys. J.* **833** 179
[14] Zegers R G T *et al* 2008 *Phys. Rev.* C **77** 024307
[15] Gupta S, Brown E F, Schatz H, Möller P and Kratz K 2007 *Astrophys. J.* **662** 1188
[16] Schatz H *et al* 2013 *Nature* **505** 12757
[17] Goriely S, Bauswein A, Just O, Pllumbi E and Janka H-T 2015 *Mon. Not. R. Astron. Soc.* **452** 3894
[18] Cole A L *et al* 2012 *Phys. Rev.* C **86** 015809
[19] Noji S *et al* 2014 *Phys. Rev. Lett.* **112** 252501
[20] Noji S *et al* 2015 *Phys. Rev.* C **92** 024312
[21] Scott M *et al* 2014 *Phys. Rev.* C **90** 025801
[22] Taddeucci T N, Goulding C A, Carey T A, Byrd R C, Goodman C D, Gaarde C, Larsen J, Horen D, Rapaport J and Sugarbaker E 1987 *Nucl. Phys.* A **469** 125
[23] Zegers R G T *et al* 2007 *Phys. Rev. Lett.* **99** 202501

[24] Zegers R G T *et al* 2006 *Phys. Rev.* C **74** 024309
[25] Langanke K and Martínez-Pinedo G 2000 *Nucl. Phys.* A **673** 481
[26] Langanke K, Kolbe E and Dean D J 2001 *Phys. Rev.* C **63** 032801
[27] Fuller G M, Fowler W A and Newman M J 1980 *Astrophys. J.* **42** 447
[28] Fuller G M, Fowler W A and Newman M J 1982 *Astrophys. J.* **252** 715
[29] Fuller G M, Fowler W A and Newman M J 1982 *Astrophys. J.* **48** 279
[30] Fuller G M, Fowler W A and Newman M J 1985 *Astrophys. J.* **293** 1
[31] Oda T, Hino M, Muto K, Takahara M and Sato K 1994 *At. Data Nucl. Data Tables* **56** 231
[32] Langanke K and Martínez-Pinedo G 2001 *At. Data Nucl. Data Tables* **79** 146
[33] Poves A, Sánchez-Solano J, Caurier E and Nowacki F 2001 *Nucl. Phys.* A **694** 157
[34] Honma M, Otsuka T, Brown B A and Mizusaki T 2002 *Phys. Rev.* C **65** 061301
[35] Honma M, Otsuka T, Brown B A and Mizusaki T 2004 *Phys. Rev.* C **69** 034335
[36] Honma M, Otsuka T, Brown B A and Mizusaki T 2005 *Eur. Phys. J.* A **25** 299
[37] Juodagalvis A and Dean D J 2005 *Phys. Rev.* C **72** 024306
[38] Möller P, Nix J R, Myers W D and Swiatecki W J 1995 *At. Data Nucl. Data Tables* **59** 185
[39] Nabi J-U and Klapdor-Kleingrothaus H V 2004 *At. Data Nucl. Data Tables* **88** 237
[40] Paar N, Colò G, Khan E and Vretenar D 2009 *Phys. Rev.* C **80** 055801
[41] Dzhioev A A, Vdovin A I, Ponomarev V Y, Wambach J, Langanke K and Martínez-Pinedo G 2010 *Phys. Rev.* C **81** 015804
[42] Niu Y F, Paar N, Vretenar D and Meng J 2011 *Phys. Rev.* C **83** 045807
[43] Dean D J, Langanke K, Chatterjee L, Radha P B and Strayer M R 1998 *Phys. Rev.* C **58** 536
[44] Juodagalvis A, Langanke K, Hix W R, Martínez-Pinedo G and Sampaio J M 2010 *Nucl. Phys.* A **848** 454
[45] Raduta A R, Gulminelli F and Oertel M 2017 *Phys. Rev.* C **95** 025805
[46] Langanke K and Martínez-Pinedo G 2003 *Rev. Mod. Phys.* **75** 819
[47] Pruet J and Fuller G M 2003 *Astrophys. J. Suppl. Ser.* **149** 189
[48] O'Connor E 2015 *Astrophys. J. Suppl. Ser.* **219** 24
[49] O'Connor E and Ott C D 2010 *Class. Quantum Grav.* **27** 114103
[50] Holt A, Engeland T, Hjorth-Jensen M and Osnes E 2000 *Phys. Rev.* C **61** 064318
[51] Lipoglavšek M *et al* 2002 *Phys. Rev.* C **65** 021302
[52] Brown B A and Rykaczewski K 1994 *Phys. Rev.* C **50** R2270
[53] Macfarlane M H 1986 *Phys. Lett.* B **182** 265
[54] Brown B A, Etchegoyen A, Godwin N S, Rae W D M, Richter W A, Ormand W E, Warburton E K, Winfield J S, Zhao L and Zimmerman C H The Oxford-Buenos-Aires-MSU shell-model code OXBASH *NSCL Report No.* MSUCL-1289 National Superconducting Cyclotron Laboratory, Michigan State University
[55] Gaarde C *et al* 1981 *Nucl. Phys.* A **369** 258
[56] Gaarde C 1985 *Proc. Niels Bohr Centennial Conference on Nuclear Structure, Copenhagen* (Amsterdam: North-Holland) p 449c
[57] Brown B A and Wildenthal B H 1988 *Annu. Rev. Nucl. Part. Sci.* **38** 29
[58] Martínez-Pinedo G, Poves A, Caurier E and Zuker A P 1996 *Phys. Rev.* C **53** R2602
[59] Juodagalvis A, Sampaio J M, Langanke K and Hix W R 2008 *J. Phys. G: Nucl. Part. Phys.* **35** 014031
[60] Woosley S E and Weaver T A 1995 *Astrophys. J. Suppl. Ser.* **101** 181
[61] Steiner A W, Hempel M and Fischer T 2013 *Astrophys. J.* **774** 17
[62] Hempel M and Schaffner-Bielich J 2010 *Nucl. Phys.* A **837** 210
[63] Dohmann H *et al* 2008 *Phys. Rev.* C **78** 041602
[64] Raywood K J *et al* 1990 *Phys. Rev.* C **41** 2836
[65] Sakai H and Sato K 2004 *Nucl. Phys.* A **731** 105
[66] Yako K *et al* 2005 *Phys. Lett.* B **615** 193
[67] Miki K *et al* 2017 *Phys. Lett.* B **769** 339